Title

Effect of Off-Target Binding on 18F-Flortaucipir Variability in Healthy Controls Across the Life Span

Journal

Journal of Nuclear Medicine, 60(10)

ISSN

0161-5505

Authors

Baker, Suzanne L
Harrison, Theresa M
Maass, Anne
et al.

Publication Date

2019-10-01

DOI

10.2967/jnumed.118.224113

Peer reviewed

Journal of Nuclear Medicine, published on March 15, 2019 as doi:10.2967/jnumed.118.224113

Effect of off-target binding on ^{18}F-Flortaucipir variability in healthy controls across the lifespan

Running title:

^{18}F-Flortaucipir in aging healthy controls

Authors:

Suzanne L Baker[1], Theresa M Harrison[2], Anne Maass[2,3], Renaud La Joie[4], William J Jagust[1,2]

Author affiliation:

1. Lawrence Berkeley National Laboratory, Berkeley, USA

2. Helen Wills Neuroscience Institute, University of California, Berkeley, Berkeley, USA

3. German Center for Neurodegenerative Diseases, Magdeburg, Germany

4. Memory and Aging Center, University of California, San Francisco, San Francisco, USA

Corresponding Author

Name: Suzanne L Baker

Address:

Lawrence Berkeley National Laboratory

1 Cyclotron Rd MS55R0121

Berkeley, California 94720

Telephone number: 510-486-4166

Fax number: 510-486-7027

Email address: slbaker@lbl.gov

Word count (4962/5000 words)

Disclosures and Financial support: This research was supported by NIH grant AG034570. Suzanne Baker serves as a consultant to Genentech. William Jagust serves as a consultant to Bioclinica, Genentech, Novartis, and Biogen. No other potential conflicts of interest relevant to this article exist.

ABSTRACT

Measuring early tau accumulation is important in studying aging and Alzheimer's disease (AD) and is only as accurate as the signal to noise ratio of the tracer. Along with aggregated tau in the form of neurofibrillary tangles, ^{18}F-Flortaucipir (^{18}F-FTP) has been reported to bind to neuromelanin, monoamine oxidase, calcification, iron, lepto-meningeal melanocytes, and microhemorrages. Although ^{18}F-FTP successfully differentiates healthy controls (HC) from subjects with AD, variability exists in the cortical signal in amyloid-β negative (Aβ-) HCs. We aimed to explore the relationship between off-target binding signal and variability in the cortical signal in HCs. Subjects (n=139) received a ^{11}C-PIB and ^{18}F-FTP-PET scan, and MRI MPRAGE. PET frames were realigned and coregistered to the MRI, and MRIs were segmented using Freesurfer. In $HC_{A\beta-}$ subjects (n=90, age range=21-94), 7 non-specific or off-target binding regions were considered: caudate, pallidum, putamen, thalamus, cerebellar white, hemispheric white, and choroid plexus. These ROIs were assigned to 3 similarly behaving groups using principle component analysis, exploratory factor analysis and Pearson correlations: 1. caudate, putamen and pallidum, (also correlated with age), 2. thalamus and white matter, 3. choroid plexus. In $HC_{A\beta-}$ subjects with ^{11}C-PIB and ^{18}F-FTP scans, correlations were calculated between white and gray matter before and after partial volume correction (PVC). The correlation between white and gray matter disappeared after PVC in ^{11}C-PIB (r^2=0.19 to 0), but persisted for ^{18}F-FTP (r^2=0.84 to 0.27), demonstrating that the correlation between white and gray matter signal in ^{18}F-FTP is not solely due to partial volume effects. A linear regression showed that off-target signal from

putamen and thalamus together explained 64% of the variability in the cortical signal in $HC_{A\beta-}$ (not seen in $HC_{A\beta+}$). Variability in $HC_{A\beta-}$, but not $HC_{A\beta+}$, correlated with an age-related off-target signal, which could be related to iron load as well as white matter signal. The noise in the ^{18}F-FTP measurement could pose challenges when studying early tau accumulation.

Keywords: tau, ^{18}F-Flortaucipir PET, off-target binding

INTRODUCTION

Accumulation of the tau protein as neurofibrillary tangles and the β-amyloid protein as plaques is the hallmark of Alzheimer's disease (AD), and also occurs in some healthy controls (HCs). Studying these proteins in vivo is important in understanding aging and AD. The typical pattern of tau deposition in brain aging and dementia has been well established in autopsy studies (*1*). The use of positron emission tomography (PET) with radiopharmaceuticals that bind to tau permits longitudinal in vivo investigations of tau deposition across the lifespan.

^{18}F-Flortaucipir (^{18}F-FTP; also known as T807 and ^{18}F-AV-1451) is a PET tracer that binds with high affinity to paired helical filament tau in neurofibrillary tangles (*2,3*). ^{18}F-FTP scans differentiate between HC and AD subjects and parallel Braak stage neurological tau progression (*4-8*). ^{18}F-FTP scans have shown that tau accumulation is mostly restricted to the medial temporal lobe in healthy controls (*9*), unless cortical β-amyloid is present, when the tracer is found in isocortical regions (*5-7*). Yet there is wide variability in ^{18}F-FTP Standardized Uptake Value Ratios (SUVRs) from amyloid-β negative healthy controls ($HC_{A\beta-}$) in regions outside the medial temporal lobes (*10*). Although ^{18}F-FTP demonstrates great promise as a clinical and research tool, off-target binding (OFF), or ^{18}F-FTP signal where aggregated tau is not expected, may complicate image interpretation (*11,12*). We hypothesized that variability in ^{18}F-FTP signal seen in cortical regions outside of the medial temporal lobes in $HC_{A\beta-}$ could be related to OFF.

Examples of ^{18}F-FTP-OFF include binding in caudate, putamen, pallidum and thalamus (*4,13*) seen in healthy controls, where tau accumulation should not occur

until late AD stages. These regions also have different ^{18}F-FTP tracer kinetics than cortical regions (*13-16*), further supporting the idea that the ligand binds to targets other than pathological tau in these regions.

Iron accumulation and age correlate with ^{18}F-FTP in the basal ganglia in HCs (*17*) making iron or ferritin possible source of ^{18}F-FTP-OFF. ^{18}F-FTP also binds to neuromelanin, which increases with age (*18,19*). Neuromelanin plays a role in the sequestration of iron and is found in lower concentrations in the cerebellum than cortical regions (*20*). Although ^{3}H-FTP binds to monoamine oxidase A (MAO-A) and B (MAO-B) in vitro (*21*), in vivo studies have yet to replicate ^{18}F-FTP binding to MAO-A or MAO-B (*22*). Both exist in lower concentrations in the cerebellum than cortex (*23*). Also, there was no significant difference in the ^{18}F-FTP OFF in the basal ganglia between Parkinson's disease patients receiving MAO-B inhibitors and those who were not (*22*). Many targets have been postulated to explain the binding of ^{18}F-FTP in the choroid plexus (ChPlex) (*19,24*), although a difference in ^{18}F-FTP-ChPlex between African American and Caucasian subjects suggests ^{18}F-FTP could be binding to neuromelanin (*25*). Lastly, variability in hemispheric white matter (HemiW) signal was reported in HCs as minor displaceable binding (*19*), leading us to classify white matter (WM) as an OFF region.

To summarize, ^{18}F-FTP-OFF has been reported in caudate, putamen, pallidum, thalamus, ChPlex and HemiW. In ^{18}F-FTP imaging in $HC_{A\beta-}$, a range of 0.5 SUVR units has been reported in the cortex (*10*). OFF could account for variability in cortical ^{18}F-FTP in $HC_{A\beta-}$. We explored the relationship between OFF and cortical

binding in $HC_{A\beta-}$ and amyloid positive HCs ($HC_{A\beta+}$) in order to better understand the variability in the ^{18}F-FTP SUVR values.

MATERIALS AND METHODS

Subjects

HC subjects (n=139; Table 1) were recruited from the Berkeley Aging Cohort Study for ^{18}F-FTP scans (132 of 139 subjects also had a ^{11}C-PIB scan to determine amyloid status). Berkeley Aging Cohort Study eligibility required that subjects were living independently in the community, performed normally on neuropsychological exams, were taking no medications that interfered with cognition, had no medical conditions that affected cognition, and had no contraindications to MRI or PET exams. The Institutional Review Board of Lawrence Berkeley National Laboratory (LBNL) approved this study; all subjects signed a written informed consent.

PET Acquisition

At LBNL, ^{11}C-PIB and ^{18}F-FTP were synthesized at the Biomedical Isotope Facility; subjects were scanned on a Siemens Biograph TruePoint PET/CT. A CT was performed at the start of each emission scan for attenuation correction. For ^{11}C-PIB, subjects were injected with 555 MBq at the start of the emission scan. Subjects were scanned for 90 minutes, frames were binned as 4x15, 8x30, 9x60, 2x180, 10x300, and 2x600 seconds. For ^{18}F-FTP, subjects were injected with 370 MBq, and the emission scan was acquired 75-115 minutes post-injection. Data were collected in listmode, allowing 80-100 minutes to be reconstructed as 4x5minute frames. PET

data were reconstructed using an ordered subset expectation maximization algorithm with attenuation and scatter correction and a 4mm Gaussian kernel.

MRI Acquisition

Subjects received a high-resolution T1-weighted magnetization prepared rapid gradient echo (MPRAGE) scan (TR/TE=2110,3.58ms, FA=15°, 1x1x1mm resolution) on a 1.5T Siemens Magnetom Avanto scanner at LBNL. MRI data were used to define ROIs for image analysis.

Data Processing

MPRAGEs were segmented using FreeSurfer v5.3 (http://surfer.nmr.mgh.harvard.edu/). All coregistration and realignment steps were performed using SPM12 (http://www.fil.ion.ucl.ac.uk/spm/software/spm12/). ^{18}F-FTP individual frames were realigned to create a mean, which was then coregistered to the subjects' MPRAGE.

All ^{18}F-FTP analyses used SUVRs with an inferior cerebellar gray matter reference region (*26*), except for an analysis examining the stability of the cortex, OFF-ROIs, and reference region. Data were partial volume corrected (PVC) using a geometric transfer matrix approach (*26,27*) using a combination of Freesurfer ROIs, extracortical hotspots, and SPM12 segmentions for CSF, skull and meninges. Both non-partial volume corrected data (non-PVC) and PVC data were analyzed. Mean SUVRs of HemiW, cerebellar white matter (CereW), caudate, pallidum, putamen,

thalamus, ChPlex, cortical ROIs grouped as Braak-stage regions (*28*), and whole cortex (composite of Braak-stage ROIs) were calculated. Braak I was defined as Freesurfer-segmented entorhinal cortex; II was hippocampus; III was parahippocampal gyrus, fusiform gyrus, amygdala and lingual gyrus; IV was middle and inferior temporal cortices, temporal pole, insula, and anterior, posterior and isthmus cingulate gyrus; V was frontal cortex, lateral occipital cortex, parietal cortex, precuneus, banks of superior temporal sulcus, accumbens, and superior and tranverse temporal cortices; VI was pericalcarine, precentral, paracentral and postcentral gyrus, and cuneus.

For ^{11}C-PIB data, the first 5 minutes of data were summed and subsequent frames were realigned to the first 5 minutes of data. Data were coregistered to the MPRAGE. To determine if subjects were $HC_{A\beta+}$ or $HC_{A\beta-}$, Logan graphical analysis DVRs (*29*) were calculated (35-90min; reference region=cerebellar gray). The ^{11}C-PIB index was calculated using the weighted mean of FreeSurfer-derived prefrontal, parietal, lateral temporal and cingulate cortices. HCs without a ^{11}C-PIB scan and under 50 years old or with ^{11}C-PIB DVR<1.065 were considered $HC_{A\beta-}$ (*30,31*).

Statistical Comparisons

Associations between OFF-ROIs and with Age in $HC_{A\beta-}$. Pearson correlations (r^2) were calculated on ^{18}F-FTP SUVRs in order to determine which OFF regions of interest (OFF-ROIs) were correlated with each other or with age. Age was included in these analyses because possible targets for OFF (iron, MAO-B) are correlated with

age. OFF-ROIs were caudate, pallidum, putamen, thalamus, HemiW, CereW and ChPlex. The grouping of OFF-ROIs was also examined with exploratory factor analysis (EFA) and principle components analysis (PCA). These analyses were done only in the $HC_{A\beta-}$ subjects (n=90; non-PVC and PVC) in order to minimize the likelihood of on-target binding of ^{18}F-FTP to tau, especially outside of medial temporal lobe. As expected, EFA and PCA confirmed the grouping patterns revealed by Pearson correlations; these ROIs were grouped together for future analyses.

$HC_{A\beta+}$>$HC_{A\beta-}$. Differences between $HC_{A\beta-}$ (age 55-95) and $HC_{A\beta+}$ for ^{18}F-FTP SUVRs in Braak ROIs and OFF-ROIs were tested using analysis of covariance (ANCOVA, controlling for age and gender). Partial eta^2 (η_p^2), the portion of variance accounted for by the amyloid status, were calculated.

Correlations between Age/OFF-ROIs and Braak ROIs. In order to define the proportion of OFF that might be included in cortical ROIs, Pearson correlations (r^2) were calculated between ^{18}F-FTP SUVRs in individual OFF-ROIs (and age) and whole cortex, Braak I, II, III/IV, and V/VI ROIs. This was done separately in $HC_{A\beta-}$ and $HC_{A\beta+}$ groups. Significance of correlations were Bonferroni corrected for multiple comparisons.

Multiple Linear Models in $HC_{A\beta-}$. Multiple linear models were fit using SUVRs from an ROI from each of the OFF-ROI groups to model the variability in the whole cortex and individual Braak ROIs. This resulted in an adjusted r^2 as well as betas and p-values for OFF-ROIs for each model. This was done separately in $HC_{A\beta-}$ and $HC_{A\beta+}$ groups.

Is Cortical Variability being driven by Variability in the Reference Region?

Without arterial sampling data, it is difficult to conclude whether the variability in the cortical SUVRs is due to actual cortical variability or due to variability in the reference region. To explore this, mean, standard deviation and coefficient of variation of ^{18}F-FTP Standard Uptake Values (SUVs) were calculated in OFF and Braak-ROIs in $HC_{A\beta-}$.

Is Cortical Variability being driven by White Matter Variability and Partial Volume Effects (PVEs)?

Because we found that ^{18}F-FTP signal in cortex and HemiW are correlated, we investigated whether this was related to PVE, shared OFF, or both by comparing WM and cortical signal in ^{11}C-PIB and ^{18}F-FTP SUVR images before and after PVC in the same subjects ($HC_{A\beta-}$ subjects; n=83). Since PVEs should be similar for ^{11}C-PIB and ^{18}F-FTP, comparison of the effect of PVC for these 2 tracers should provide some evidence for how much of the binding is related to PVE and how much is related to shared binding to targets.

For this comparison, ^{11}C-PIB scans were processed using an approach similar to the one applied to the ^{18}F-FTP data. ^{11}C-PIB SUVRs were calculated from 50-70min, the data were PVCed using the same set of ROIs as ^{18}F-FTP and inferior cerebellar gray was the reference region. Means of HemiW, CereW and cortex were calculated with and without PVC. Pearson correlations (r^2) were calculated between cortical tracer binding and HemiW and CereW for ^{18}F-FTP and ^{11}C-PIB SUVRs (non-PVC and PVC).

RESULTS

^{18}F-FTP Retention is Highly Variable in HC$_{A\beta-}$

Fig. 1 demonstrates the variability seen across HC$_{A\beta-}$ subjects. Even in subjects younger than 40 who should have no global cortical tau accumulation (*32*), the whole cortical SUVR shows considerable variability, ranging from 0.85-1.19 (non-PVC) and 0.86-1.23 (PVC).

Associations between OFF-ROIs and with Age in HC$_{A\beta-}$

Pearson intercorrelations (r^2) between all OFF-ROI SUVRs and between each OFF-ROI and age in all HC$_{A\beta-}$ subjects are shown for both non-PVC and PVC (Table 2) data. Age and ^{18}F-FTP binding in caudate, pallidum and putamen are highly correlated with one another (non-PVC r^2>0.4, PVC r^2>0.5) and were also grouped into one factor (EFA) and component (PCA) (Supplemental Table 1-2). SUVR in thalamus is weakly correlated with caudate, putamen and pallidum, but more highly correlated with HemiW and CereW. Thalamus and WM were also grouped together using EFA and PCA. The higher correlations seen in HemiW with caudate, pallidum, and putamen for non-PVC data are most likely due to PVEs, demonstrated by lower r^2 for PVC correlations. Lastly, ^{18}F-FTP binding in ChPlex significantly correlated with thalamus before PVC, and with nothing after PVC. Results from Pearson correlations, PCA and EFA support the 3 different groups of OFF-ROIs: 1. age, caudate, pallidum and putamen (the age-related group), 2. thalamus, HemiW and CereW, and 3. ChPlex.

$HC_{A\beta+}$>$HC_{A\beta-}$

Fig. 2 shows the comparison between $HC_{A\beta-}$ and $HC_{A\beta+}$ for Braak and OFF-ROIs. There was no significant difference in ^{18}F-FTP SUVR OFF-ROIs between $HC_{A\beta+}$ and $HC_{A\beta-}$ when controlling for age and gender (non-PVC and PVC; amyloid status $\eta_p^2 \leq 0.06$). There was a significant difference in ^{18}F-FTP SUVR for all Braak ROIs between $HC_{A\beta+}$ and $HC_{A\beta-}$ subjects.

Age/OFF-to-Braak ROIs

We next investigated relationships between age, OFF-ROIs and cortical ^{18}F-FTP binding by performing Pearson correlations for non-PVC (Figs. 3A and 3B) and PVC SUVRs (Figs. 3C and 3D) in $HC_{A\beta-}$ (Figs. 3A and 3C) and $HC_{A\beta+}$ (Figs. 3B and 3D). Within $HC_{A\beta-}$ subjects, correlations of cortical binding with OFF-ROIs decrease after PVC, but remain significant, demonstrating that PVEs alone cannot explain the correlations. All correlations in $HC_{A\beta+}$ are lower than in $HC_{A\beta-}$ subjects. In $HC_{A\beta+}$, Braak II (hippocampus) has the highest correlations with OFF-ROIs, however none are significant after PVC. Predictably, in $HC_{A\beta+}$ HemiW has significant correlations with Braak II-VI before PVC, but nothing is significant after PVC.

Multiple Linear Models

Whole cortex showed the strongest correlations after PVC with putamen (from the age-related OFF-ROIs) and thalamus (from the WM and thalamus OFF-ROIs). Therefore we used putamen, thalamus and ChPlex as independent measures and whole cortex and Braak ROIs as dependent measures with a series of multiple

linear models to explore how well OFF accounted for cortical variability in $HC_{A\beta-}$ subjects. The betas and adjusted r^2 are reported in Table 3 for Braak I, II, III/IV, V/VI and whole cortex. The betas are the weights for putamen, thalamus, and ChPlex in the linear model resulting in the r^2 with the Braak ROI or whole cortex as the dependent variable. For example, the linear equation for PVC whole cortex=0.1*putamen+0.33*thalamus+0.01*ChPlex. To put the betas into perspective, the mean SUVR in $HC_{A\beta-}$ subjects for putamen was 1.47±0.29 (non-PVC) and 1.54±0.35 (PVC), thalamus was 1.24±0.18 (non-PVC and PVC) and ChPlex was 1.15±0.22 (non-PVC) and 2.78±0.94 (PVC). A lower amount of variability was explained in Braak I (adjusted r^2=0.30 and 0.22 for non-PVC and PVC) in comparison to other Braak regions. ChPlex was only significant when explaining variability in the signal for the hippocampus (Braak II). Thalamus was significant ($p<0.01$) in explaining SUVR for all Braak ROIs. Putamen was significant ($p<0.001$) in explaining Braak III/IV, V/VI and whole cortex (PVC), and Braak II (non-PVC, $p<0.01$).

Multiple linear models were also performed in $HC_{A\beta+}$ (data not shown). Only the linear model for Braak II resulted in a significant ($p<0.001$) adjusted r^2 (non-PVC=0.59, PVC=0.31); thalamus and ChPlex significantly contributed to the model.

Is Cortical Variability being driven by Variability in the Reference Region?

Whether the cortical variability was driven by reference region in ^{18}F-FTP was explored by calculating the coefficient of variation of SUVs in $HC_{A\beta-}$ subjects, shown in Supplemental Table 3. Coefficient of variation was similar across regions,

but was smallest in the inferior cerebellar gray; the mean and standard deviation of SUV was smallest in the inferior cerebellar gray, leading us to believe that inferior cerebellar gray is a sufficient reference region and is not the cause of the cortical variability.

Is Cortical Variability Being Driven by WM Variability and PVEs?

The PVEs of WM on cortical gray were explored by comparing the correlation between WM (HemiW and CereW) and cortical gray in ^{18}F-FTP SUVR before and after PVC. We decided to examine both HemiW and CereW because CereW does not suffer from PVEs from whole cortex. To gauge the degree of correlation expected due to PVEs, the analysis was also done in ^{11}C-PIB SUVRs in the same subjects. The analysis was limited to $HC_{A\beta-}$ subjects in order to minimize any on-target binding. Fig. 4 shows the corresponding HemiW versus mean of whole cortex for the 83 subjects. ^{11}C-PIB correlations between HemiW and whole cortex changed from r^2=0.19 to 0 as a result of PVC (CereW correlations with cortex also went from r^2=0.19 to 0), demonstrating that PVC can remove the correlation between white and gray matter signal. However, PVC did not remove the correlations between white and gray matter signal in ^{18}F-FTP; HemiW to whole cortex r^2=0.84 for non-PVC and decreased to 0.27 as a result of PVC (^{18}F-FTP CereW to whole cortex went from r^2=0.57 to 0.23 after PVC). All correlations between gray and white were significant at $p<0.001$ except for PVC ^{11}C-PIB.

DISCUSSION

^{18}F-FTP is a useful tracer to examine pathological tau load differences between HCs and subjects with AD. However, in $HC_{A\beta-}$, where tau paired helical filaments are unlikely to be found in substantial numbers in the neocortex (*33*,*34*), there is variability in cortical signal (*10*) which makes measuring early tau deposition challenging. We showed that 64% of the cortical signal variability in our $HC_{A\beta-}$ subjects can be explained by signal from OFF-ROIs (Table 3). Furthermore, the mean cortical ^{18}F-FTP variability in $HC_{A\beta-}$ subjects has a SUVR range of 0.5 SUVR units, and is similar in $HC_{A\beta-}$ subjects younger than 40 years old (these subjects have a low likelihood of having neocortical tau (*33,34*)). Similar variability in $HC_{A\beta-}$ ^{18}F-FTP cortical signal was also shown in 422 $HC_{A\beta-}$ subjects (*10*).

There is a possibility that there is little variability in Braak ROI SUVRs in $HC_{A\beta-}$ subjects and the variability seen stems from the reference region. In attempt to determine if variability in the reference region could be driving this, we calculated SUVs for $HC_{A\beta-}$. The reference region, inferior cerebellar gray, had the lowest coefficient of variation of SUVs of all the ROIs. The inferior cerebellar gray is no more or less stable than other regions. It has been shown that the cerebellum has a similar distribution volume (calculated using arterial sampling data) between HCs and subjects with AD (*16*), implying a certain level of stability. However it has also been shown that the distribution volume calculated from arterial input function correlates with age (with different slopes) in both the cerebellum and in cortical regions (*15*).

The 3 OFF-ROI groups were an age-related group (which included caudate, pallidum and putamen), a WM group (which included thalamus), and ChPlex. The age-related group could be driven by binding to neuromelanin or iron. Iron load (quantified using MRI R_2*) has been shown to correlate with ^{18}F-FTP binding in the basal ganglia and age in HCs and ADs (*17*); additionally, in HCs, pallidum and putamen have been reported to have higher iron than other ROIs, which we also observed for ^{18}F-FTP in our $HC_{A\beta-}$ cohort. The age-related off-target contribution to variability in cortical signal is relatively small.

The WM group of OFF ROIs contributed more to the variability in the cortical signal than the age-related group in a multiple linear regression. Correlations between CereW and Braak ROIs were similar to correlations between HemiW to Braak ROIs after PVC. CereW and Braak ROIs are not proximal and therefore do not contribute to each others' PVEs, implying that the correlations between WM and Braak ROIs are not solely driven by PVEs. We further explored the possibility that PVEs drive the cortical signal variability in ^{18}F-FTP by looking at the relationship between WM and whole cortex in ^{18}F-FTP and ^{11}C-PIB scans before and after identical PVC approaches. We showed that ^{11}C-PIB WM signal could be removed from cortical signal using PVC, but a correlation between WM and cortical signal persisted after PVC in ^{18}F-FTP scans. This suggests the correlation between the WM and gray matter signal is a real feature of ^{18}F-FTP binding properties and not the result of PVEs. WM explains substantial variance of signal in the cortex of the $HC_{A\beta-}$. It is unclear what ^{18}F-FTP could be binding to in WM although the lipophilic of β-sheet binding tracers may explain this finding.

ChPlex did not significantly correlate to any OFF-ROI or age, except thalamus before PVC (not significant after PVC). ChPlex only significantly correlated with hippocampus non-PVC SUVR in $HC_{A\beta-}$ and $HC_{A\beta+}$ and PVC SUVR in $HC_{A\beta-}$, and only significantly contributed to the multiple linear model predicting hippocampal SUVR. Although ChPlex makes quantification of hippocampus SUVR challenging, the OFF in this region does not correlate with other OFF-ROIs or Braak regions outside of hippocampus. Along with hippocampus being steeped in PVEs, it is also known to have automated segmentation problems (*8*). Segmentation inaccuracies would negatively impact the precision of non-PVC and PVC quantification. Hippocampus ^{18}F-FTP signal should be interpreted with caution.

PVEs are not the only source of the variability in ^{18}F-FTP signal in $HC_{A\beta-}$, nor did our PVC algorithm create correlations where none existed. The correlations between cortex and WM existed in both non-PVC and PVC data, and most correlations between cortical and OFF-ROIs decreased as a result of PVC. The agreement between non-PVC and PVC results leads us to conclude that the OFF in the cortical regions is not an artifact of data analysis.

Focusing on only the $HC_{A\beta-}$ subjects, OFF-ROIs account for less of the signal variance in Braak I (entorhinal cortex) than other Braak regions. Because entorhinal cortex is the site of earliest accumulation of tau in HCs, this is most likely due to true binding of ^{18}F-FTP to tau in subjects in this region. In contrast, >50% of cortical signal variability could be explained by OFF-ROIs in $HC_{A\beta-}$ subjects.

In $HC_{A\beta+}$ subjects, OFF-ROIs were only significant predictors of hippocampal ^{18}F-FTP signal. There is a significant difference between $HC_{A\beta+}$ and $HC_{A\beta-}$ subjects'

Braak ROI SUVRs but no significant difference in OFF-ROI SUVRs. When correlating OFF-ROIs to Braak ROIs in $HC_{A\beta+}$ subjects, there were few significant correlations in the non-PVC data (save hippocampus, HemiW, and caudate), and no significant correlations after PVC. These two results lead us to conclude that ^{18}F-FTP is binding to tau in $HC_{A\beta+}$ subjects. The ratio of on-target binding to OFF in $HC_{A\beta+}$ subjects seems to be high enough such that the OFF-ROI correlations are not significant. However, it could be interesting as a future direction to quantify the relative amounts of on and OFF in $HC_{A\beta+}$ subjects.

It is beyond the scope of this paper to analyze the variability of the OFF-ROI and Braak signal within subject, longitudinally. It has been shown that using HemiW as a reference region for longitudinal tau data reduced variability and enhanced discrimination between diagnostic cohorts (*35*). The success of the HemiW reference region could be partly related to covariance of HemiW and gray matter, and therefore normalizing by HemiW would remove that white-matter-related off-target signal from the gray matter.

CONCLUSION

Although ^{18}F-Flortaucipir has been shown to track tau deposition in the brain, off target binding increases variability in the cortical signal in amyloid negative healthy controls. There are three main ROI groups with related off target binding signal: an age-related group including the caudate, pallidum and putamen, a white matter-related group including the thalamus, and lastly the choroid plexus.

This variability is correlated to a signal likely related to iron deposition, as well as the amount of ^{18}F-Flortaucipir measured in the white matter. PVEs do not completely account for the variability in the cortical signal. The variability in signal in healthy controls related to off-target binding should be considered when studying the earliest deposition of tau using ^{18}F-Flortaucipir. Either the sample size should be sufficient to account for the variability across subjects or possibly controlling for measurements of off-target binding when correlating ^{18}F-Flortaucipir measurements with other neuroimaging or cognitive measure could result in improved sensitivity.

REFERENCES

1 Braak H, Braak, E. Neuropathological stageing of Alzheimer-related changes. *Acta neuropathol*. 1991;82:239-59.

2 Chien DT, Bahri S, Szardenings AK, et al. Early clinical PET imaging results with the novel PHF-tau radioligand [F-18]-T807. *J Alzheimers Dis*. 2013;34:457-68.

3 Xia CF, Arteaga J, Chen G, et al. [(18)F]T807, a novel tau positron emission tomography imaging agent for Alzheimer's disease. *Alzheimers Dement*. 2013;9:666-76.

4 Johnson KA, Schultz A, Betensky RA, et al. Tau positron emission tomographic imaging in aging and early Alzheimer disease. *Ann neurol*. 2016;79:110-9.

5 Scholl M, Lockhart SN, Schonhaut DR, et al. PET imaging of tau deposition in the aging human brain. *Neuron*. 2016;89:971-82.

6 Schwarz AJ, Yu P, Miller BB, et al. Regional profiles of the candidate tau PET ligand 18F-AV-1451 recapitulate key features of Braak histopathological stages. *Brain.* 2016;139:1539-50.

7 Wang L, Benzinger TL, Su Y, et al. Evaluation of tau imaging in staging Alzheimer disease and revealing interactions between beta-amyloid and tauopathy. *JAMA neurol*. 2016;73:1070-77.

8 Ossenkoppele R, Rabinovici G, Smith R. Discriminative accuracy of [18F]flortaucipir positron emission tomography for Alzheimer disease vs other neurodegenerative disorders. *JAMA*. 2018;320:1151-62.

9 Schultz SA, Gordon BA, Mishra S, et al. Widespread distribution of tauopathy in preclinical Alzheimer's disease. *Neurobiol aging*. 2018;72:177-85.

10 Lowe VJ, Wiste HJ, Senjem ML, et al. Widespread brain tau and its association with ageing, Braak stage and Alzheimer's dementia. *Brain*. 2018;141:271-87.

11 Sander K, Lashley T, Gami P, et al. Characterization of tau positron emission tomography tracer [(18)F]AV-1451 binding to postmortem tissue in Alzheimer's disease, primary tauopathies, and other dementias. *Alzheimers dement*. 2016;12:1116-24.

12 Barrio JR. The irony of PET tau probe specificity. *J Nucl Med*. 2018;59:115-16.

13 Baker SL, Lockhart SN, Price JC, et al. Reference tissue-based kinetic evaluation of 18F-AV-1451 for tau imaging. *J Nucl Med*. 2017;58:332-8.

14 Shcherbinin S, Schwarz AJ, Joshi A, et al. Kinetics of the tau PET tracer 18F-AV-1451 (T807) in subjects with normal cognitive function, mild cognitive impairment, and Alzheimer disease. *J Nucl Med*. 2016;57:1535-42.

15 Barret O, Alagille D, Sanabria S, et al. Kinetic modeling of the tau PET tracer (18)F-AV-1451 in human healthy volunteers and Alzheimer disease subjects. *J Nucl Med*. 2017;58:1124-31.

16 Golla SSV, Timmers T, Ossenkoppele R, et al. Quantification of tau load using [(18)F]AV1451 PET. *Mol Imaging Biol*. 2017;19:963-71.

17 Choi JY, Cho H, Ahn SJ, et al. Off-Target (18)F-AV-1451 binding in the basal ganglia correlates with age-related iron accumulation. *J Nucl Med*. 2018;59:117-20.

18 Marquie M, Normandin MD, Vanderburg CR, et al. Validating novel tau positron emission tomography tracer [F-18]-AV-1451 (T807) on postmortem brain tissue. *Ann Neurol*. 2015;78:787-800.

19 Lowe VJ, Curran G, Fang P, et al. An autoradiographic evaluation of AV-1451 tau PET in dementia. *Acta neuropathol Commun*. 2016;4:58.

20 Zecca L, Bellei C, Costi P, et al. New melanic pigments in the human brain that accumulate in aging and block environmental toxic metals. *Proc Natl Acad Sci USA*. 2008;105:17567-72.

21 Vermeiren C, Motte P, Viot D, et al. The tau positron-emission tomography tracer AV-1451 binds with similar affinities to tau fibrils and monoamine oxidases. *Mov Disord*. 2018;33:273-81.

22 Hansen AK, Brooks DJ, Borghammer P. MAO-B inhibitors do not block in vivo Flortaucipir([(18)F]-AV-1451) binding. *Mol Imaging Biol*. 2018;20:356-60.

23 Tong J, Meyer JH, Furukawa Y, et al. Distribution of monoamine oxidase proteins in human brain: implications for brain imaging studies. *J Cereb Blood Flow Metab*. 2013;33:863-71.

24 Marquie M, Verwer EE, Meltzer AC, et al. Lessons learned about [F-18]-AV-1451 off-target binding from an autopsy-confirmed Parkinson's case. *Acta neuropathol Commun*. 2017;5:75.

25 Lee CM, Jacobs HIL, Marquie M, et al. 18F-Flortaucipir binding in choroid plexus: related to race and hippocampus signal. *J Alzheimers Dis*. 2018;62:1691-702.

26 Baker SL, Maass A, Jagust WJ. Considerations and code for partial volume correcting [18F]-AV-1451 tau PET data. *Data Brief*. 2017;15:648-57.

27 Rousset OG MY, Evans AC. Correction for partial volume effects in PET: principle and validation. *J Nucl Med*. 1998;39:904-11.

28 Maass A, Landau S, Baker SL, et al. Comparison of multiple tau-PET measures as biomarkers in aging and Alzheimer's disease. *Neuroimage*. 2017;157:448-63.

29 Logan J FJ, Volkow ND, Wang GK, Ding YS, Alexoff DL. Distribution volume ratios without blood sampling from graphical analysis of PET data. *J Cereb Blood Flow Metab.* 1996;16:834-40.

30 Mormino EC, Brandel MG, Madison CM, et al. Not quite PIB-positive, not quite PIB-negative: slight PIB elevations in elderly normal control subjects are biologically relevant. *Neuroimage*. 2012;59:1152-60.

31 Villeneuve S, Rabinovici GD, Cohn-Sheehy BI, et al. Existing Pittsburgh Compound-B positron emission tomography thresholds are too high: statistical and pathological evaluation. *Brain*. 2015;138:2020-33.

32 van Bergen JMG, Li X, Quevenco FC, et al. Low cortical iron and high entorhinal cortex volume promote cognitive functioning in the oldest-old. *Neurobiol Aging*. 2018;64:68-75.

33 Braak H, Thal DR, Ghebremedhin E, Del Tredici K. Stages of the pathologic process in Alzheimer disease: age categories from 1 to 100 years. *J Neuropathol Exp Neurol*. 2011;70:960-9.

34 Braak H, Braak, E. Frequency of stages of Alzheimer-related lesions in different age categories. *Neurobiol Aging*. 1997;18:351-7.

35 Southekal S, Devous MD, Sr., Kennedy I, et al. 18F-Flortaucipir quantitation using a parametric estimate of reference signal intensity (PERSI). *J Nucl Med*. 2017;59:944-51.

TABLE 1

Age range	n	Gender (M/F)	MMSE	Years Education	Amyloid group	Has PIB scan
20-35	14	12/2	29±1.2*	15.5±1.4**	Aβ-	9
35-55	5	4/1	29.2±1.8	17.2±1.8	Aβ-	3
55-75	24	10/14	29.0±1.2	17.8±1.7	Aβ-	24
75-95	47	18/29	29.0±1.0	16.9±1.8	Aβ-	47
55-95	49	20/29	28.5±1.4	16.5±1.8	Aβ+	49

Subjects: No significant difference between $HC_{A\beta-}$ and $HC_{A\beta+}$ in MMSE or education. *One subject missing MMSE. **Two subjects missing years of education.

TABLE 2

	Caudate	Pallidum	Putamen	Thalamus	HemiW	CereW	ChPlex
Age	0.42** 0.57**	0.64** 0.55**	0.68** 0.71**	0.30** 0.12	0.13 0.00	0.15* 0.01	0.03 0.12
Caudate		0.72** 0.59**	0.77** 0.83**	0.67** 0.41**	0.58** 0.13	0.55** 0.18**	0.11 0.08
Pallidum			0.92** 0.66**	0.69** 0.40**	0.55** 0.21**	0.56** 0.25**	0.07 0.10
Putamen				0.68** 0.38**	0.52** 0.10	0.51** 0.13	0.06 0.08
Thalamus					0.79** 0.61**	0.79** 0.66**	0.21** 0.02
HemiW						0.83** 0.83**	0.11 0.01
CereW							0.09 0.02

Positive correlations (r^2) between age and OFF-ROIs. Top number is r^2 between non-PVC data, bottom is PVC data. **p<0.001, *p<0.01, corrected for multiple comparisons.

TABLE 3

	Independent Variable Betas			
Dependent Variable	Putamen	Thalamus	ChPlex	Adjusted r^2
Braak I Non-PVC	-0.02	0.34*	0	0.22**
Braak I PVC	0.16	0.38*	0.01	0.30**
Braak II Non-PVC	0.14*	0.39**	0.26**	0.82**
Braak II PVC	0.07	0.42**	0.07**	0.55**
Braak III/IV Non-PVC	0.03	0.38**	-0.01	0.66**
Braak III/IV PVC	0.11**	0.31**	0.01	0.64**
Braak V/VI Non-PVC	-0.07	0.49**	-0.03	0.55**
Braak V/VI PVC	0.09**	0.33**	0.01	0.61**
Whole Cortex Non-PVC	-0.04	0.46**	-0.02	0.60**
Whole Cortex PVC	0.10**	0.33**	0.01	0.64**

A series of multiple linear models (run in $HC_{A\beta}$-) with FTP SUVRs in cortical ROIs as dependent measure, and SUVRs in putamen, thalamus and ChPlex as independent measures. ** $p<0.001$, * $p<0.01$.

FIGURE 1

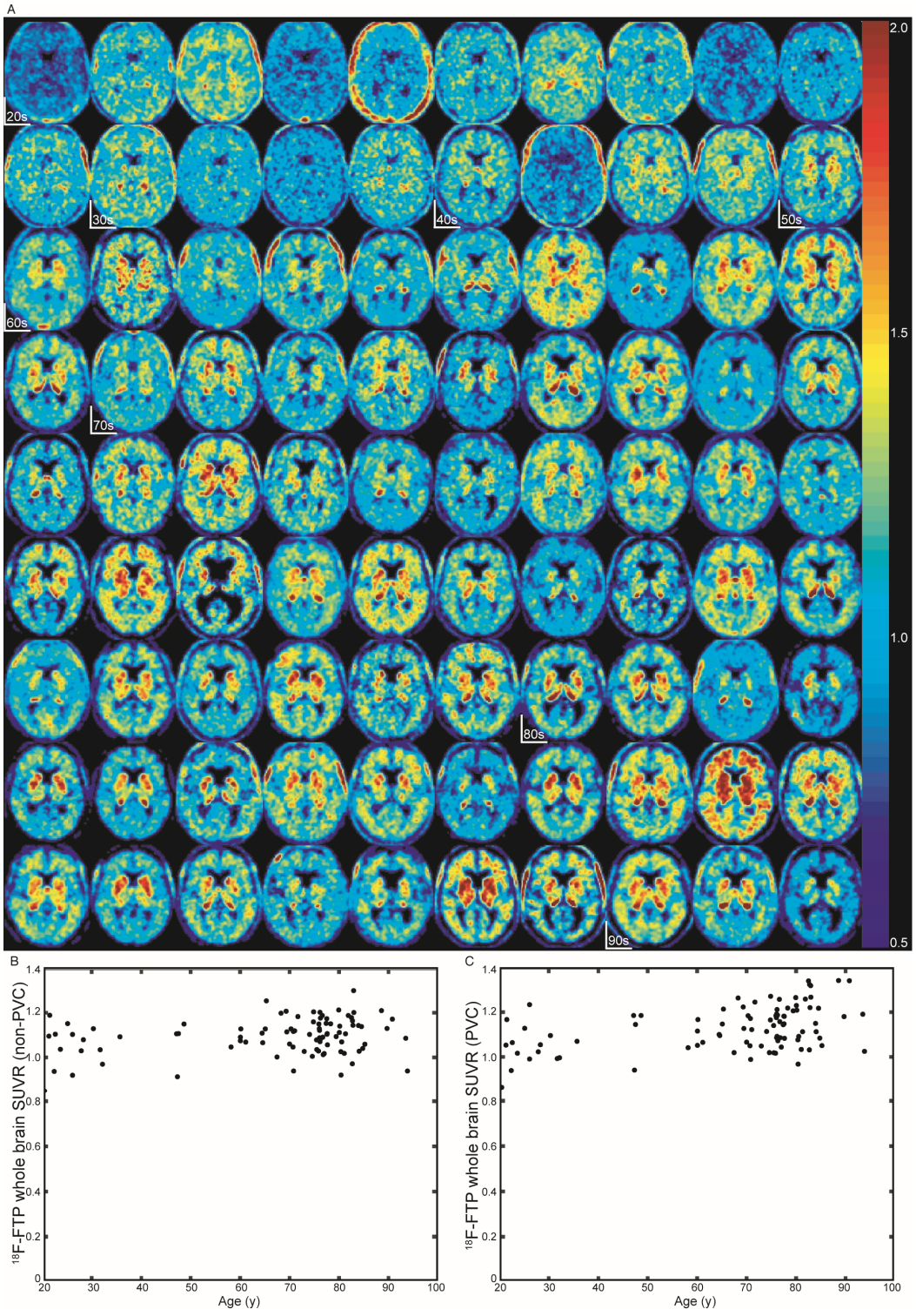

High variability in $HC_{A\beta-}$. A: ^{18}F-FTP SUVR images in MNI space in order of age. The start of each age decade is marked. B: age versus non-PVC whole cortical SUVR (r^2=0.06, $p<0.05$), C: age versus PVC whole cortical SUVR (r^2=0.18, $p<0.001$).

FIGURE 2

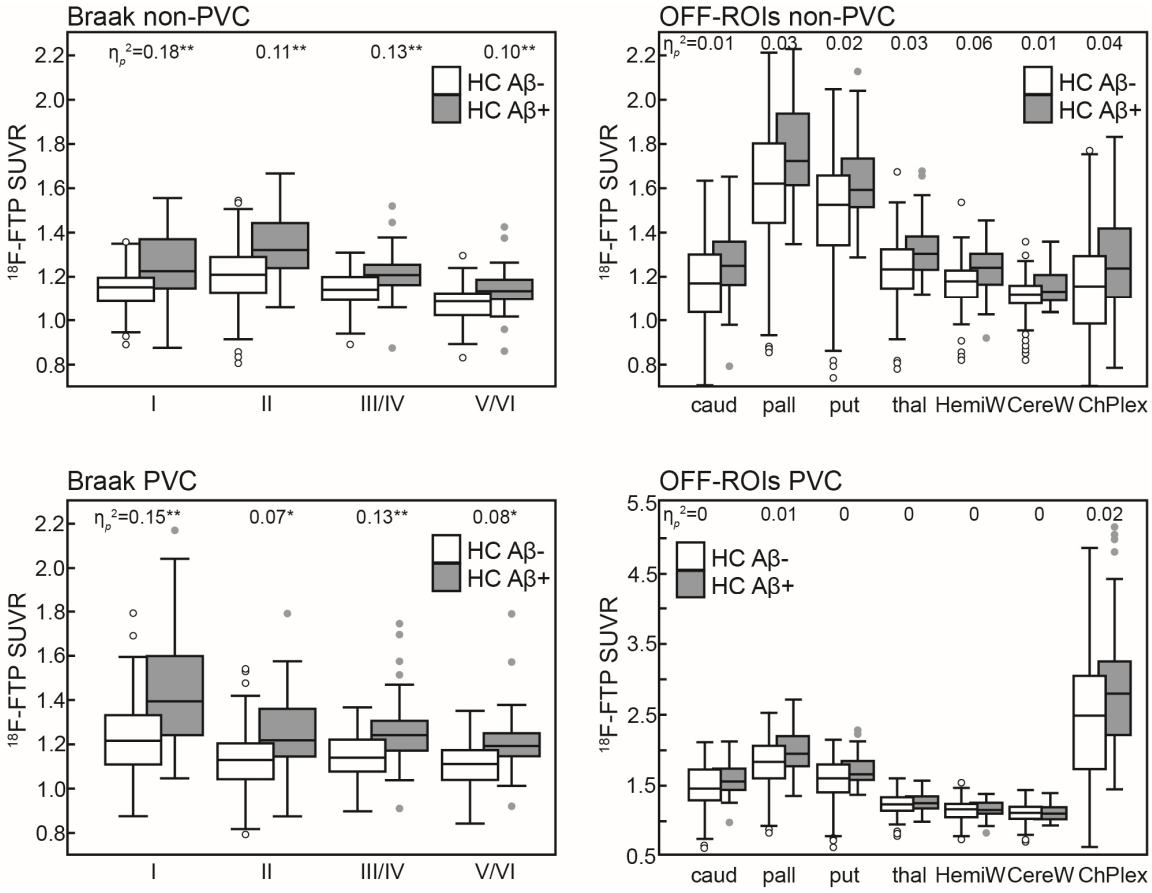

Central mark indicates median, top and bottom of the box indicate 75th and 25th percentile, whisker extent=median±1.57(75th percentile – 25th percentile)/sqrt(number subjects), "o" represents subjects beyond the whisker extent. Significance of p<0.005 (*) and p<0.001 (**) denoted for η_p^2.

FIGURE 3

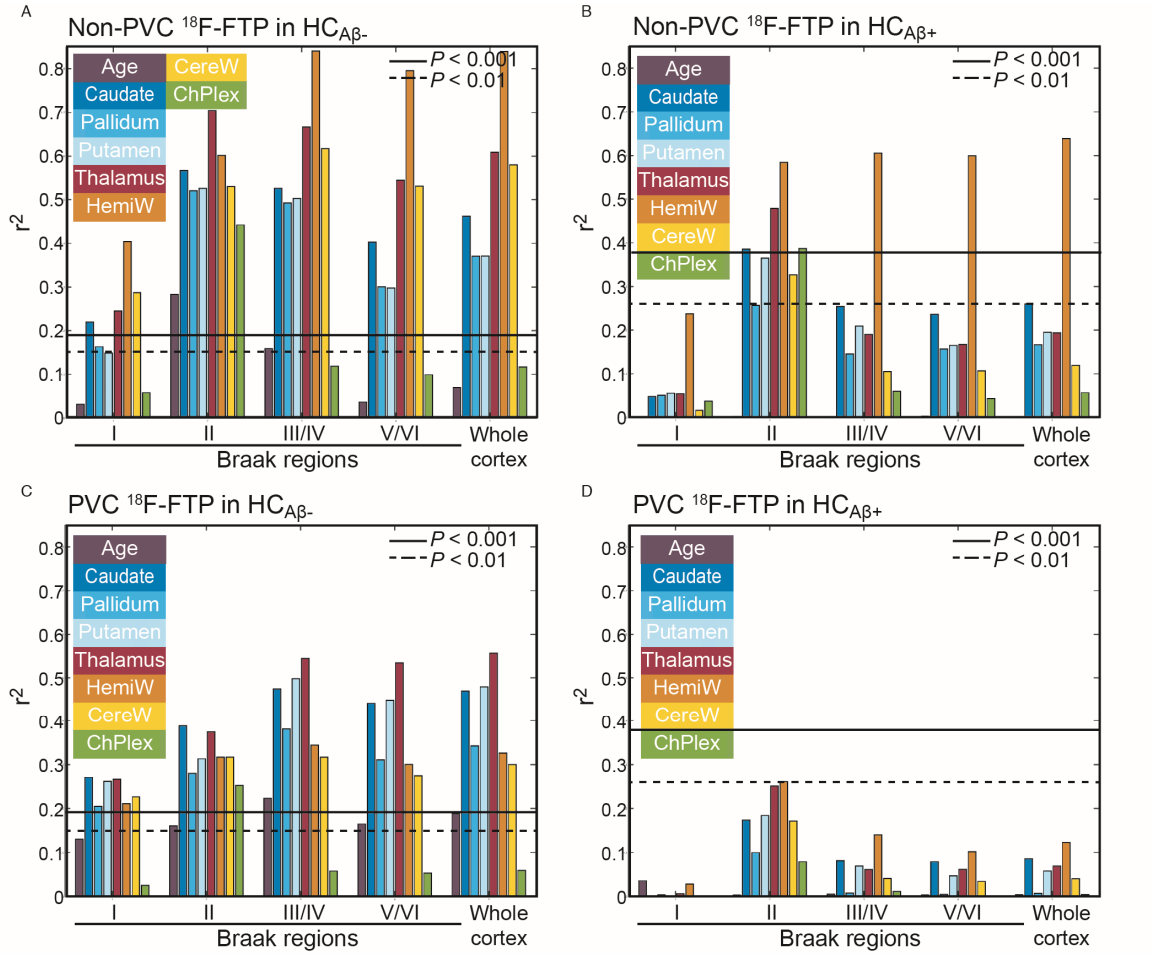

Pearson r^2 between ^{18}F-FTP SUVR in cortical regions, age and OFF-ROIs. P-values were Bonferroni corrected.

FIGURE 4

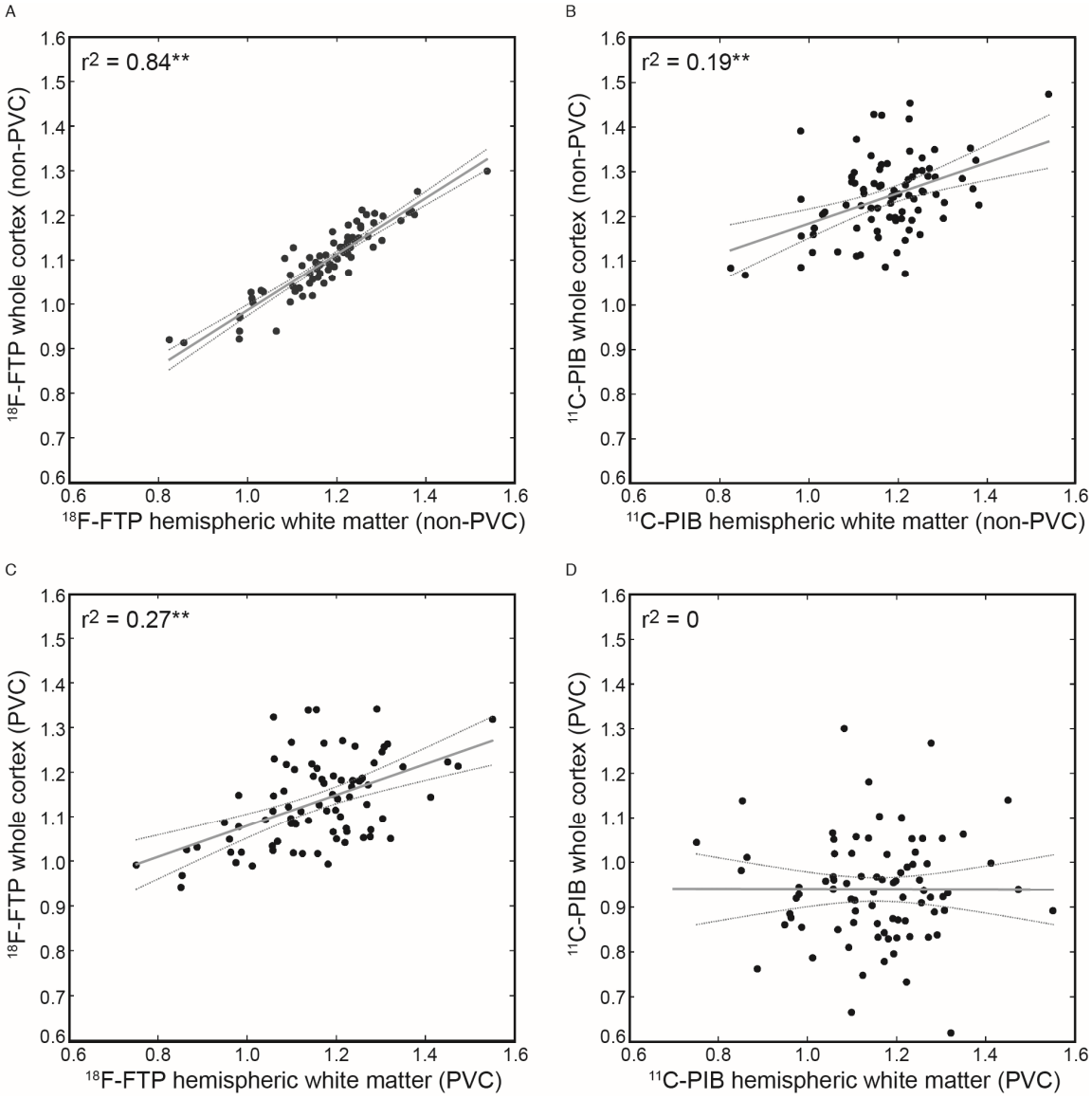

Correlations between HemiW and whole cortex SUVRs. A: Non-PVC ^{18}F-FTP, B: non-PVC ^{11}C-PIB, C: PVC ^{18}F-FTP, D: PVC ^{11}C-PIB. Gray line: linear model fit, dashed gray lines: 95% confidence interval.

Supplemental Material

Supplemental Table 1

	Factors for non-PVC data				Factors for PVC data			
	1	2	3	Uniq	1	2	3	Uniq
Lcaud	0.659			0.184	0.899			0.150
Rcaud	0.705			0.194	0.908			0.157
Lpall	0.942			0.054	0.716			0.273
Rpall	0.915			0.078	0.689			0.308
Lput	1.021			0.022	0.989			0.050
Rput	1.054			0.013	1.024			0.031
Lthal		0.770		0.039		0.756		0.118
Rthal		0.716		0.076		0.704		0.193
HemiW		0.976		0.118		0.980		0.134
Cerew		1.008		0.110		0.979		0.094
Lchoroid			0.820	0.166			0.886	0.125
Rchoroid			0.958	0.145			0.912	0.203

Factor loadings from Exploratory Factor Analysis (EFA; Jamovi: https://www.jamovi.org/) on non-PVC and PVC data in $HC_{A\beta-}$ subjects using oblimin rotation, thresholded loadings at 0.5. The number of factors based on parallel analysis. Uniqueness (Uniq) is the proportion of common variance of the variable not associate with other factors. Left caudate (Lcaud), right caudate (Rcaud), left pallidum (Lpall), right pallidum (Rpall), left putamen (Lput), right putamen (Rput) make up the first factor. The second factor is made up of left thalamus (Lthal), right thalamus (Rthal), hemispheric white matter (HemiW), and cerebellar white matter (CereW). The third factor was made up of left choroid plexus (Lchoroid) and right choroid plexus (Rchoroid).

Supplemental Table 2

	Variance explained	ROIs in component
PCA component 1	66.9%	Choroid plexus
PCA component 2	25.5%	Caudate, pallidum, putamen
PCA component 3	3.8%	Thalamus, Hemispheric white, Cerebellar white

Components from Principle Components Analysis (PCA; Matlab R2015a: https://www.mathworks.com). Only first 3 components are reported since remaining components contribute <3%.

Supplemental Table 3

	SUV Mean (g/mL)	SUV Standard Deviation	SUV Coefficient of Variation
Inferior cerebellar gray	**0.46**	**0.15**	**0.32**
Caudate	**0.55**	**0.23**	**0.41**
Pallidum	**0.76**	**0.32**	**0.42**
Putamen	**0.70**	**0.30**	**0.42**
Thalamus	**0.58**	**0.23**	**0.39**
Eroded HemiW	**0.55**	**0.20**	**0.36**
CereW	**0.52**	**0.19**	**0.36**
Braak 1	**0.53**	**0.18**	**0.34**
Braak 2	**0.57**	**0.21**	**0.38**
Braak 3	**0.53**	**0.18**	**0.34**
Braak 4	**0.53**	**0.18**	**0.34**
Braak 5	**0.51**	**0.17**	**0.34**
Braak 6	**0.48**	**0.16**	**0.33**

Standard Uptake Value (SUVs; SUV=PET concentration [Bq/mL] x weight [g] / injected radiotracer [Bq])) was calculated in $HC_{A\beta-}$ subjects non-PVC data. HemiW: Hemispheric white, CereW: cerebellar white. Eroded HemiW means a binary HemiW mask was smoothed to the scanner resolution and all voxels>0.7 comprised the eroded HemiW mask.

The Journal of NUCLEAR MEDICINE

Effect of off-target binding on ^{18}F-Flortaucipir variability in healthy controls across the lifespan

Suzanne L Baker, Theresa M Harrison, Anne Maaß, Renaud La Joie and William Jagust

J Nucl Med.
Published online: March 15, 2019.
Doi: 10.2967/jnumed.118.224113

The Journal of Nuclear Medicine is published monthly.
SNMMI | Society of Nuclear Medicine and Molecular Imaging
1850 Samuel Morse Drive, Reston, VA 20190.
(Print ISSN: 0161-5505, Online ISSN: 2159-662X)

SNMMI SOCIETY OF NUCLEAR MEDICINE AND MOLECULAR IMAGING